Biosensors and Bioelectronics ■ (■■■■) ■■■–■■■

Contents lists available at ScienceDirect

Biosensors and Bioelectronics

journal homepage: www.elsevier.com/locate/bios

Graphene-titanium dioxide nanocomposite based hypoxanthine sensor for assessment of meat freshness

Jasmine A.V Albelda [a,b,1], Aytekin Uzunoglu [a], Gil Nonato C. Santos [b], Lia A. Stanciu [a,*]

[a] School of Materials Engineering, Purdue University, 701 West Stadium Avenue, West Lafayette, IN 47907, USA
[b] Physics Department, De La Salle University, 2401 Taft Avenue, Manila 1004, Philippines

ARTICLE INFO

Article history:
Received 30 November 2015
Received in revised form
3 March 2016
Accepted 17 March 2016

Keywords:
Hypoxanthine
Xanthine oxidase
Biosensor
Graphene/TiO_2 nanocomposite
Meat freshness

ABSTRACT

We report on the fabrication of a graphene/titanium dioxide nanocomposite (TiO_2-G) and its use as an effective electrode material in an amperometric hypoxanthine (Hx) sensor for meat freshness evaluation. The nanocomposite was characterized by TEM, XRD, FTIR, XPS, TGA, BET, and CV using the redox couples $[Fe(CN)_6]^{-3/-4}$ and $[Ru(NH_3)_6]^{+3/+2}$ respectively. The TiO_2/G nanocomposite offered a favorable microenvironment for direct electrochemistry of xanthine oxidase (XOD). The fabricated Nafion/XOD/TiO_2-G/GCE sensor exhibited excellent electro catalytic activity towards Hx with linear range of 20 μM to 512 μM, limit of detection of 9.5 μM, and sensitivity of 4.1 nA/μM. In addition, the biosensor also demonstrated strong anti-interference properties in the presence of uric acid (UA), ascorbic acid (AA) and glucose. Minimal interference of xanthine (Xn) was observed at ~7%. Moreover, the biosensor showed good repeatability (4.3% RSD) and reproducibility (3.8% RSD). The reported biosensor was tested towards the detection of Hx in pork tenderloins stored at room temperature for seven days. There was a good correlation ($r=0.9795$) between biosensor response and measurements obtained by a standard enzymatic colorimetric method. The TiO_2-G nanocomposite is therefore an effective electrode material to be used in electrochemical biosensors to assess the freshness of meat.

1. Introduction

Obtaining reliable information on meat quality, which would ultimately provide a guaranteed quality of meat products for consumers, is one of the challenges facing the meat industry. Meeting this challenge requires fast and accurate techniques for objective measurement of meat quality traits such as freshness. However, determining meat freshness is rather complex in that it includes different microbiological, physicochemical and biochemical attributes related to two different processes – (1) aging, which is determined by the period of storage that meat needs in order to reach the optimum state of consumption and (2) meat spoilage because of bacterial growth and/or by enzymatic actions (Dave and Ghaly, 2011; Gil et al., 2011).

Traditionally, there have been two methods to evaluate meat freshness; one consists of a sensory test controlling organoleptic features with the help of experts and the other is the chemical or biochemical determination of the concentration of target bio-indicators (Gil et al., 2011). While the former method has proved to be rapid, it is also expensive and at times less reliable since it is difficult for this method to evaluate slight differences in meat freshness before the initial stage of degradation. The latter method has attracted a large number of studies that tried to relate the freshness of meat with the concentration or the presence of certain substances such as biogenic amines, trimethylamine, volatile amines, degradation products of ATP and bacterial count. Typical gas sensors, e-nose and e-tongue devices detect the presence of amines (Galgano et al., 2009; Önal, 2007; Vinci and Antonelli, 2002) and correlate it with the meat freshness while most electrochemical sensors detect a particular ATP degradation product such as Hx (Ag et al., 2006; Baş et al., 2014; Lawal and Adeloju, 2012a, 2012b; Liu et al., 2013; Luong and Male, 1992; Yao, 1993; Zhang et al. 2010b) and Xn (Devi et al., 2013a, 2011a, 2011b; Lawal and Adeloju, 2012b; Öztürk et al., 2014; Shan et al., 2009). Biogenic amines however, are released at higher concentrations on the later part of meat degradation as compared to Hx or Xn which is known to accumulate right after the animal is slaughtered (Hernández-Cázares et al., 2010; Watanabe et al., 1986; Yam et al., 1995; Yano et al., 1996). Particularly linked to the presence of Hx is the suggestion that it causes a bitter taste which is easy to identify in the degrading fish or meat (Lawal and Adeloju, 2012a).

* Corresponding author.
E-mail addresses: gil.santos@dlsu.edu.ph (G.N.C. Santos), lstanciu@purdue.edu (L.A. Stanciu).
[1] Albelda, JAV is also affiliated with the Philippine Normal University, Taft Avenue, Manila, Philippines.

http://dx.doi.org/10.1016/j.bios.2016.03.041
0956-5663/

Hx can be determined using classical methods such as spectrophotometric (Amigo et al., 2005; Weeranantanaphan et al., 2011) and chromatographic (Akaoka et al., 1975; Cooper et al., 2006; Rong et al., 2015; Vallé et al., 1998) measurements. These methods, in general, are time consuming, expensive and require skilled persons to operate the necessary apparatus. The use of biosensors has many advantages over these classical methods in terms of simplicity, sensitivity, faster analysis and lower cost.

In this study, an Hx sensor was developed using a hydrothermally synthesized graphene-titanium dioxide (TiO_2-G) nanocomposite as platform for the immobilization of the enzyme, XOD. Due to its good biocompatibility and high conductivity, TiO_2 has been widely used in the fabrication of electrochemical biosensors. In these biosensors, TiO_2 was employed as support matrix for immobilizing enzymes, which can facilitate the direct electron transfer and enhance the catalytic activity of enzyme (Fan et al., 2011a, 2011b, Feng et al., 2013; Yu et al., 2013; Zhou et al., 2006). Graphene as well, has shown excellent performance not only in direct electrochemistry of enzymes, but also in electrochemical detection of small biomolecules and electroanalysis (Hu et al., 2015; Shao et al., 2010). The combination of graphene and other nanoparticles may have a synergistic effect on the unique physicochemical properties of the resulting nanocomposite (Lim et al., 2012). The TiO_2-G nanocomposite reported here could provide a suitable microenvironment for the development of enzyme sensors with excellent electrochemical sensing properties particularly towards Hx and for the accurate and reliable evaluation of meat freshness.

There are only a few XOD biosensors based on composites containing metal oxides or based on graphene modified electrodes and most of them detect Xn instead of Hx. Some of these studies include graphene sheets functionalized with water soluble copolymer (Zhang et al., 2010b) and phosphonic acid-functionalized silica nanoparticles (Liu et al., 2013) for Hx detection, electrochemically reduced graphene oxide for the simultaneous determination of UA, Xn and Hx in blood serum and urine (Raj and John, 2013), and zinc oxide nanoparticle/chitosan/multiwalled carbon nanotube/polyaniline composite film (Devi et al., 2012) and zinc oxide nanoparticles–polypyrrole composite film (Devi et al., 2011a) for Xn detection. However, to the best of our knowledge, none of the reported studies used the simple configuration used herein: XOD immobilized in TiO_2-G nanocomposite.

2. Material and methods

2.1. Reagents, materials and equipment

XOD from bovine milk (E.C. 1.17.3.2, lyophilized powder), titanium isopropoxide ($Ti(O^iPr)_4$ or TTIP), N,N-Dimethylformamide (DMF), Hx, phosphate buffer saline solutions (PBS), nafion (5% solution), sodium dodecyl sulfate (SDS), potassium ferricyanide ($K_3Fe(CN)_6$), Hexaammineruthenium(III) chloride ($Ru(NH_3)_6Cl_3$), and other reagents were purchased from Sigma Aldrich. All solutions were prepared using deionized water ($\sim$18 MΩ cm). Graphene (98% carbon) was obtained from ACS Material and used as received without further modification.

The morphological and structural characterizations of the nanocomposite were carried out using transmission electron microscopy (TEM, SEI Tecnai G230) and X-ray diffraction (XRD, Bruker D8). Attenuated Total Reflectance - Fourier Transform Infrared Spectroscopy (ATR-FTIR) spectra were recorded using Perkin Elmer Spectrum 100 ATR-FTIR. A Kratos Axis Ultra DLD spectrometer equipped with monochromatic Al Kα (1486.6 eV) excitation source was employed to collect the XPS data of the prepared samples. The XPS results were calibrated using the main C1s peak (284.6 eV) (Uzunoglu et al., 2015). Thermogravimetric Analysis (TGA) measurements were obtained on Q50 TGA (TA Instruments) analyzer under air atmosphere from room temperature to 800 °C at a heating rate of 10 °C/min. The surface area of the nanocomposite was determined from the nitrogen adsorption–desorption isotherms at liquid nitrogen temperature (77 K) using Tri-star Micromeritics. Prior to measurement, the sample was degassed for 4 h at 100 °C.

Electrochemical measurements were performed using Bio-Logic SAS Model SP-150. A conventional three-electrode system, which consisted of a platinum wire as counter electrode, an Ag/AgCl (saturated in NaCl) as reference electrode, and a bare or modified glassy carbon electrode (GCE-3 mm diameter, BASi) as working electrode, was used in all electrochemical experiments. Unless specified, all measurements were done in triplicate at room temperature.

2.2. Synthesis of TiO_2-G nanocomposite

The TiO_2-G nanocomposite was synthesized via a modified hydrothermal method (Anjusree et al., 2013; Fan et al., 2011a, 2011b; Muduli et al., 2009; Vasconcelos et al., 2011). In a typical preparation, 20 mg of graphene was first dispersed by sonication in a mixed solution of deionized H_2O (10 mL), ethanol (5 mL) and SDS (5 mL) for 15 min. Then, 0.1 mL of TTIP was added to the suspension and sonicated for 1 h. The resultant mixture was transferred to a 50 mL Teflon-sealed autoclave and kept in a box furnace maintained at 130 °C for 12 h. The final product was isolated by filtration using Grade 6 Whatmann filter paper (pore size 3 μm) and centrifugation at 6000 rpm for 10 min, rinsed thoroughly with a mixture of deionized water and ethanol (1:1 ratio), and dried at 80–90 °C in a dust-proof environment. For comparison, TiO_2 nanoparticles were synthesized using the same method except the absence of graphene in the mixture subjected to hydrothermal conditions.

2.3. Fabrication of Hx sensor

The prepared TiO_2-G nanocomposite (1 mg) was dispersed in DMF (1 mL) by sonication for 1 h to get a homogenous dispersion (1 mg/mL). Prior to surface modification, the GCE was polished with 0.3 μm and 0.05 μm alumina slurries, rinsed with deionized water and then sonicated in a mixture of deionized water and ethanol for a few minutes before air-drying at room temperature. Next, 16 μL of the nanocomposite suspension was drop casted onto the surface of freshly polished GCE and dried at room temperature for 1–2 h to obtain the TiO_2-G modified GCE. Then, 20 μL (0.5 U) of XOD solution was dropped onto the surface of the nanocomposite modified GCE and was allowed to dry at room temperature for 2 h. The prepared Nafion/XOD/TiO_2-G/GCE electrode was immersed in 50 mM PBS to remove the unbounded XOD. To improve the sensor stability, the surface of the electrode was coated with a thin layer (4 μL) of 5% nafion. The electrodes are stored in PBS at 4 °C when not in use.

2.4. Test and optimization of Hx sensor

The electrochemical behavior of the fabricated electrodes was studied using cyclic voltammetry (CV) in unstirred solution. For chronoamperometric measurements, the three-electrode system connected to the potentiostat/galvanostat was immersed in 5 mL of 50 mM PBS. Then, different concentrations of standard Hx solutions were added into PBS and the current generated was recorded while the reaction mixture was stirred at 200 rpm. The same procedure was followed for the testing of meat samples, except that the standard Hx solutions were replaced with filtered meat extracts.

Please cite this article as: Albelda, J.A.V, et al., Biosensors and Bioelectronics (2016), http://dx.doi.org/10.1016/j.bios.2016.03.041

To determine the optimum working conditions of the fabricated Hx sensor, the following parameters were investigated: applied potential, enzyme immobilization time, enzyme loading, the amount of nanocomposite, and buffer pH. The applied potential was varied from 0.6 to 0.9 V with an increment of 0.05 V and the current responses were recorded. Similarly, the enzyme immobilization time was investigated from 1 to 5 h with an increment of 1 h, the enzyme loading from 0.1 U to 1.0 U, the amount of nanocomposite from 5 μL to 20 μL, and buffer pH from 4.0 to 8.0.

2.5. Determination of Hx in Pork

Pork tenderloins were purchased from a local meat shop and were certified fresh. The meat samples obtained were vacuum-sealed and stored at −20 °C prior to transport and testing in the lab. The meat samples were then thawed at room temperature and allowed to degrade for 7 days at room temperature. Every 24 h, 5 mg of pork tenderloin was finely chopped and homogenized in deionized water (15 mL) using a homogenizer (IKA Ultra Turrax workstation). Then, the homogenate was centrifuged at 6000 rpm for 10–15 min and the supernatant was collected and filtered using Grade 1 Whatmann filter paper. A portion of the meat extract was stored immediately at −20 °C for subsequent use in a colorimetric assay. The content of Hx in the actual meat samples was determined by the fabricated sensor as described in Section 2.4 for its testing under optimal working conditions. The difference stayed in the replacement of the Hx solution with the meat extract. The Hx content was interpolated from the calibration curve between Hx concentrations vs. current obtained under optimal working conditions. For measurements using colorimetric method, the meat extracts stored at −20 °C were thawed at room temperature and filtered using a 10 kDa MWCO spin filter for 5 min at 12,000 rpm to remove proteins and enzymes that might interfere with the assay. The colorimetric determination of Hx concentration was obtained using an Hx/Xn colorimetric/fluorometric assay kit purchased from BioVision.

3. Results and discussion

3.1. Characterization of TiO_2-G nanocomposite

The surface morphology of the nanocomposite was studied by TEM. The surface of graphene before the hydrothermal treatment to produce TiO_2 nanoparticles is shown in Fig. 1A. The surface morphology of the TiO_2-G nanocomposite is shown in Fig. 1B and C. A layer of TiO_2 nanoparticles was successfully decorated into the basal plane of the graphene sheet after the hydrothermal treatment. The TiO_2 particles akin to the shape of spheres and globules have sizes that are in the range of 10–20 nm. Except for "wrinkling" and "buckling", the layer of graphene was not affected after the incorporation of TiO_2 nanoparticles. An unaltered structure maintains the necessary electrical conductivity for this materials' incorporation in an amperometric biosensor.

The incorporation of TiO_2 nanoparticles on the graphene substrate was verified by FTIR. Fig. S1A shows the ATR-FTIR spectra of hydrothermally synthesized titania nanoparticles, TiO_2-G nanocomposite and graphene. The appearance of $–CH_2$ (2900 cm^{-1} and 2850 cm^{-1}), $–CH_3$ (1466 cm^{-1}) and –OH (broad stretch from 3500 to 3200 cm^{-1} and peak at 1645 cm^{-1}) stretches in the spectra of TiO_2 nanoparticles and TiO_2-G nanocomposite can be attributed to the influence of SDS and adsorbed water. The Ti–O and Ti–O–Ti bonding are represented in the 800–400 cm^{-1} region (Vasconcelos et al., 2011). The slope near the 600 cm^{-1} region of the hydrothermally synthesized TiO_2 nanoparticles and the TiO_2-G nanocomposite indicates the presence of these bonds. The spectrum of graphene shows the skeletal vibration of graphene sheets at 1574 cm^{-1} and some residual C=O and C–O groups as indicated at 1745 cm^{-1} and 1154 cm^{-1} respectively (Dong et al., 2012; Murugan et al., 2010). It is interesting to note that the signature peak for the aromatic C–C of graphene also appeared in the spectrum of the synthesized nanocomposite albeit, shifted to 1554 cm^{-1}, and a peak appeared at 1116 cm^{-1} in the otherwise stretched C–O band of the graphene spectrum. This could indicate the interaction of Ti on the oxygen containing groups on the basal plane (hydroxyl and epoxide) and on the sheet edges (carboxyl groups) of graphene as a result of the hydrothermal process, which promotes the incorporation of TiO_2 into the graphene surface (Fan et al., 2011b; Muduli et al., 2009; Zhang et al., 2010a).

The surface chemistry and the chemical interaction between TiO_2 and graphene were investigated further using XPS technique. The XPS survey spectrum of TiO_2-G is shown in Fig. S2A. The peaks that appeared at 280, 460, and 530 eV, corresponding to C 1s, Ti 2p, and O 1s, respectively, confirmed the existence of Ti, O, and C. The Ti (2p) core level of the XPS spectra of the TiO2-G nanocomposite (Fig. S2B) showed two peaks centered at 459.0 eV and 464.8, which can be assigned to the binding energies of the Ti $2p_{1/2}$ and Ti $2p_{3/2}$ electrons. The presence of these intrinsic peaks confirms the successful incorporation of anatase TiO_2 on the graphene surface(Guo et al., 2016). The deconvolated C1s spectra (Fig. S3A) of graphene showed four peaks centered at 285.6, 285.9, 288.0, and 289.6 eV corresponding to the presence of C–C (C=C),

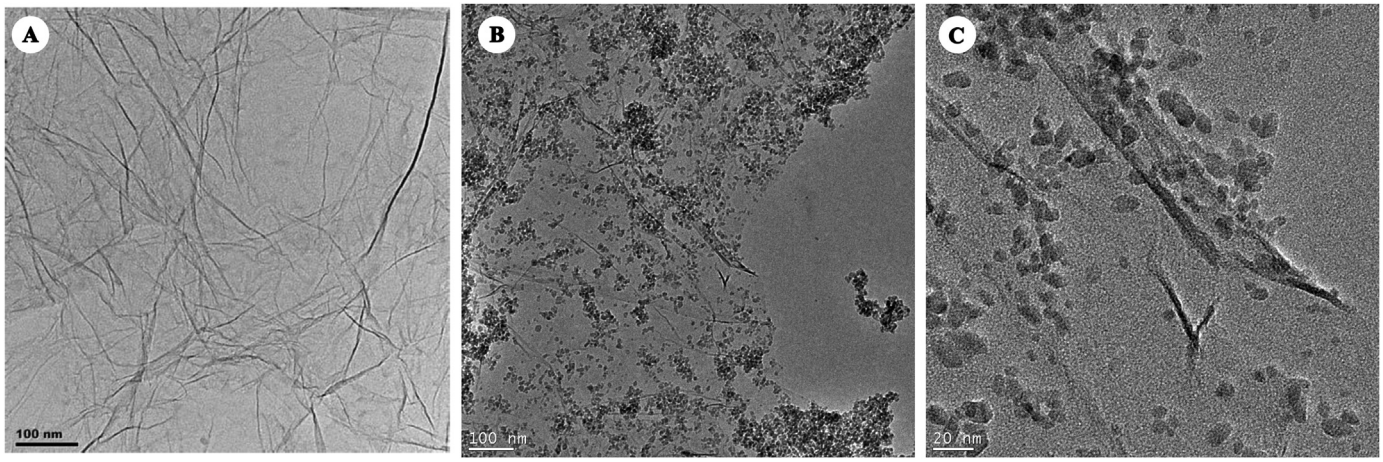

Fig. 1. TEM micrographs of (A) graphene and (B and C) TiO_2-G nanocomposite. The TEM micrograph of bare graphene was taken from the ACS Material technical data sheet (⟨http://www.acsmaterial.com/upload/122/2224235334.pdf⟩).

C-OH, C=O, and C(O)O bonds, respectively (Wang et al., 2013). While four different types of bonding were obtained from the deconvolated C1s spectra of graphene, the XPS spectra of TiO_2-G (Fig. S3B) indicated the presence of five types of chemical bonding. The peaks located at 284.6, 285.6, 288.0, and 290.8 eV are due to the sp2 carbon atoms and carbon atoms bonding with oxygenate groups while the additional peak at 283.7 eV is attributed to the formation of Ti-C bond (Akhavan and Ghaderi, 2009). The interaction between TiO_2 and graphene was also observed in the convolated O 1s spectra of TiO2-G (Fig. S4). The deconvolated O 1s spectra had four different components which are O-C, O=C, O-Ti, and Ti-O-C located at 530.2, 531.6, 532.9, and 531.1, respectively (Qiu et al., 2014). Both the XPS spectra of C 1s and O 1s confirmed the formation of the chemical bond between TiO_2 and graphene.

The XRD patterns of the synthesized TiO_2 nanoparticles, TiO_2-G nanocomposite and graphene are compared in Fig. S1B. All the peaks in the bare TiO_2 are indexed in the pure anatase form (PDF 00-001-0562). The strongest peak at 25.32^0 corresponds to the 101 plane of anatase TiO_2. This peak and other peaks characterizing anatase TiO_2 also appeared in the XRD pattern of the TiO_2-G nanocomposite. This result suggests the complete formation of anatase TiO_2 during the hydrothermal process. The diffraction peaks of graphene, however, are not distinguishable in the obtained XRD pattern. The much lower crystallinity of graphene compared to TiO_2, which results in the shielding of the graphene peaks by TiO_2, can be attributed to this observation. The observed shielding/overlapping of the TiO_2 and graphene peaks is similar to the findings of other studies on TiO_2-G nanocomposite synthesis (Anjusree et al., 2013; Guo et al., 2012; Li et al., 2014; Shen et al., 2011; Zou et al., 2011).

The nanocomposite contains about 61% titania as calculated from the obtained TGA curve. The BET surface area of the nanocomposite is 136.4 m^2/g, comparable to the surface area of TiO_2-G composite reported by Anjusree (Anjusree et al., 2013). The BET surface area of TiO_2 nanoparticles synthesized in the same hydrothermal conditions as the TiO_2-G nanocomposite is 102.6 m^2/g, which is about twice the surface area of hydrothermally synthesized TiO_2 nanoparticles in previously reported studies (Dong et al., 2012). The presence of graphene thereby increases the surface area of the nanocomposite. A greater BET surface area could be beneficial to achieve better adsorption and can supply more surface active sites for electrochemical reactions favorable to biosensor preparations.

The redox couples $[Fe(CN)_6]^{-3/-4}$ and $[Ru(NH_3)_6]^{+3/+2}$ were used as redox probe to study the electrochemical properties of the TiO_2-G nanocomposite. These are standard systems for electrode comparison because $[Fe(CN)_6]^{-3/-4}$ is surface sensitive but not oxide sensitive, while $[Ru(NH_3)_6]^{+3/+2}$ has a nearly ideal outer-sphere redox system that is insensitive to most surface defects or impurities on electrodes (Chen and McCreery, 1996; Chen et al., 2012; Tang et al., 2009). The CV data obtained for the redox probes used is shown in Table S1 and the corresponding cyclic voltammogram is shown in Fig. S5. The apparent heterogeneous electron transfer rate was determined using the method of Nicholson (Nicholson, 1965). The TiO_2-G nanocomposite showed a faster electron transfer rate in $[Fe(CN)_6]^{-3/-4}$ compared to bare GCE as indicated by its smaller peak potential difference, ΔE. The smaller ΔE of the nanocomposite (85 mV) is consistent with the calculated apparent electron transfer rate, k value of 0.0090 cm s^{-1}. The electron transfer rate of the nanocomposite in $[Ru(NH_3)_6]^{+3/+2}$ is slightly lower compared to bare GCE but the nanocomposite electrode has a more negative formal potential at -173 mV compared to bare GCE (-166 mV). An apparent increase in the oxidation and reduction current for the nanocomposite in $[Fe(CN)_6]^{-3/-4}$ and $[Ru(NH_3)_6]^{+3/+2}$ respectively as compared to bare GCE was also observed. Results indicate that TiO_2-G nanocomposite possesses the requisite surface structure and electronic properties to support the rapid electron transfer for $[Fe(CN)_6]^{3-/4-}$ and $[Ru(NH_3)_6]^{+3/+2}$. When the effect of varying the scan rate to the peak currents was investigated, it was found that the oxidation and reduction peak currents change linearly with the square root of scan rate indicating that the reaction at the electrode surface for both redox couples was controlled by diffusion.

3.2. Direct electrochemistry of XOD on Nafion/XOD/TiO_2-G/GCE electrode

Although the TiO_2-G electrode exhibits favorable apparent electron transfer rates, it may not be effective for enzyme-based electrochemical detection if it does not provide efficient electron transfer between the active center of the enzyme and the electrode. Because the active centers of most redox enzymes such as XOD are located deeply in a hydrophobic cavity of the molecule, mediators are typically required to assist the electron transfer (Urban, 2013). Such process is undesirable in some systems and sensing is typically slow. Direct electron communication between the active center of the enzyme and the electrode, which is referred to as "direct electrochemistry of enzyme", is preferred. To investigate this electrochemical property, XOD was immobilized onto the TiO_2-G nanocomposite modified GCE by physical adsorption and then subjected to CV. Cyclic voltammograms of different modified electrodes in 50 mM PBS are shown in Fig. 2A.

The absence of peak was observed in the TiO_2-G modified GCE (Fig. 2A – black solid line) in 50 mM PBS. However, a pair of well-defined redox peaks (Fig. 2A – red solid line) were observed after XOD was immobilized in the TiO_2-G modified GCE. This result indicates that XOD was successfully immobilized on the surface of

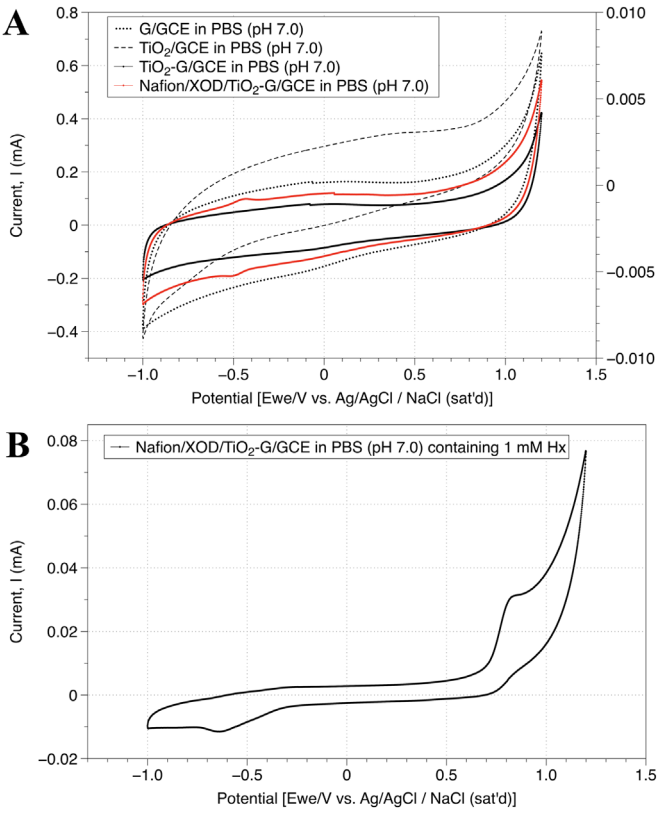

Fig. 2. Cyclic Voltammograms of (A) G/GCE, TiO_2-GCE, TiO_2-G/GCE and Nafion/XOD/TiO_2-G/GCE electrodes in 50 mM PBS of pH 7.0 and (B) Nafion/XOD/TiO_2-G/GCE electrode in 50 mM PBS of pH 7.0 containing 1 mM of Hx. Scan rate: 100 mV/s.

the nanocomposite and has undergone an oxidation-reduction process at the electrode, which further suggests a direct electron transfer between the active site of XOD and the electrode. The anodic and cathodic peak potentials were located at *ca* − 0.44 V and − 0.48 V vs. Ag/AgCl respectively. The ratio of the anodic and cathodic currents is near to one, suggesting that the redox process is quasi-reversible. The observed voltammetric characteristics are consistent with reported values for free flavin adenine dinucleotide (FAD) and enzyme-bound FAD (Rodrigues et al., 1991; Zhou et al., 2006). FAD is one of the three cofactors of XOD; the two others being molybdenum (Mo) and ferredoxin iron sulphur (Fe_2S_2). According to literature (Metz and Thiel, 2009), the mechanism of action of XOD consists of Hx being oxidized to Xn, the reduction of the oxidized form of the molybdenum center and then an intra-enzymatic electron transfer from molybdenum to FAD, followed by FAD reduction to $FADH_2$. Thus, the direct electrochemical reaction could be described as $[XOD - FAD]+2e^{-}+2H^{+} \leftrightharpoons [XOD - FADH_2]$ (Liu et al., 2013; Shan et al., 2009). The observed redox peaks must have resulted from the direct electron transfer of the immobilized enzyme due to the conversion of XOD-FAD to XOD-$FADH_2$. The TiO_2-G nanocomposite may have provided a suitable microenvironment that affected the kinetics of the electrode reaction for XOD allowing it to transfer electrons towards the underlying GCE without the aid of a mediator.

3.3. Electrochemical behavior of nanocomposite electrode to Hx

The cyclic voltammogram describing the electrochemical behavior of the Nafion/XOD/TiO_2-G modified GCE electrode when 1 mM of Hx was added in 50 mM PBS (pH 7.0) is shown in Fig. 2B. An increase in the anodic current at a potential of *ca* 0.8 V was observed pertaining to the oxidation of Hx. The reaction is catalyzed by XOD, generating hydrogen peroxide (H_2O_2) and UA, which can be described by the following equations:

$$Hx+O_2 \xrightarrow{XOD} Xn+H_2O_2$$

$$Xn+O_2 \xrightarrow{XOD} UA+H_2O_2$$

Thus, both Hx and Xn can be detected at the XOD/TiO_2-G modified electrode by measuring the oxidation current of H_2O_2.

3.4. Optimization of experimental conditions

Results of optimization experiments yield the following: optimum applied potential – 0.8 V; optimum enzyme immobilization time – 2 h; optimum enzyme loading – 0.5 U; optimum amount of TiO_2-G nanocomposite – 16 μL and; optimum buffer pH – 7.0. Subsequent amperometric measurements were done using these optimum working conditions. Details of the optimization experiments can be found in the Supplementary Information (Figs. S6–S12).

3.5. Interference studies

The relatively high applied potential (0.8 V) used in the sensor operation could potentially electro oxidize other compounds present in real meat samples such as UA or AA. This can potentially negatively affect the selectivity of the biosensor towards Hx. Thus, the effect of possible interferents such as Xn, UA, AA and glucose were investigated. As shown in Fig. 3, the presence of glucose has no interfering effect on the sensor response. UA and AA have minimal effect ($<2\%$ for $n=3$ trials) on the current response. When Xn was added, the sensor response increased by about 7% based on $n=3$ trials. This is expected since XOD catalyzes both Hx and Xn. The interference of Xn however, is relatively low. In the study of Torres (Torres et al., 2013), Xn increased the current response by 15%. In the study of Mao et al. (2001), Xn shows around 22% of the current response to Hx and as much as 10% was reported in the study of Hu (2000).

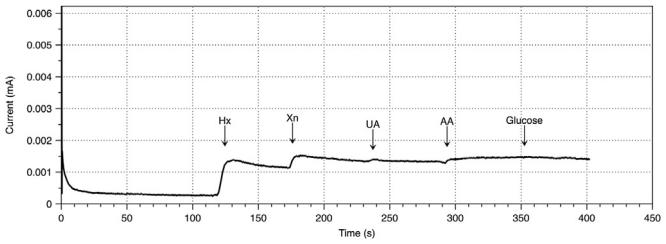

Fig. 3. Current response of the Nafion/XOD/TiO_2-G/GCE biosensor to the successive addition of 200 μM Hx, 20 μM Xn, 20 μM UA, 20 μM AA and 20 μM glucose.

3.6. Analytical performance of the Hx sensor

The amperometric response of the biosensor to Hx was determined by the successive addition of 20 μM standard concentrations of Hx to 5 mL of 50 mM PBS of pH 7.0 under optimal conditions. As shown in Fig. 4, a rapid response was recorded upon addition of Hx and a steady state was reached in less than 20 s The linear range was from 20 μM to 512 μM with correlation coefficient $R^2=0.9981$ and linear equation $y = [0.0041 \pm 0.0005]x - [0.0567 \pm 0.0188]$. The limit of detection (LOD) was calculated to be 9.5 μM and the sensitivity was 4.1 nA/μM. The detection limit was calculated based on the equation: $LOD = (\sigma/S)\bullet 3.3$ where σ is the standard deviation of the background and S is the slope of the calibration plot.

To the best of our knowledge, this study is the first to report the use of a graphene/metal oxide nanocomposite for the sensing of Hx. Moreover, since the number of literature reports on the use of graphene nanocomposite, as platform for the construction of Hx sensor is limited, the performance of the Hx sensor in this study is compared to other carbon and metal nanoparticles based sensors. The sensitivity of the fabricated Nafion/XOD/ TiO_2-G/GCE sensor (4.1 nA/μM) is higher compared to the sensor that immobilized XOD on carbon fibre microelectrodes (0.00344 nA/μM) (Mao et al., 2001) and the sensor that immobilized XOD on a glassy carbon paste electrode (1.2 nA/μM) (Timur et al., 2004). The linear range (20–512 μM) is wider compared to other reported carbon and metal nanoparticles based Hx sensors such as that of Zhang et al. (2010b), Zhang et al. (2012), Torres et al. (2013), Devi et al. (2013b), Liu et al. (2013), and Timur et al. (2004) which has a linear range of 0.03–280 μM, 1.5–35.4 μM, 10–135 μM, 0.05–150 μM, and 1–261 μM, and 20–80 μM respectively. However, the detection limits

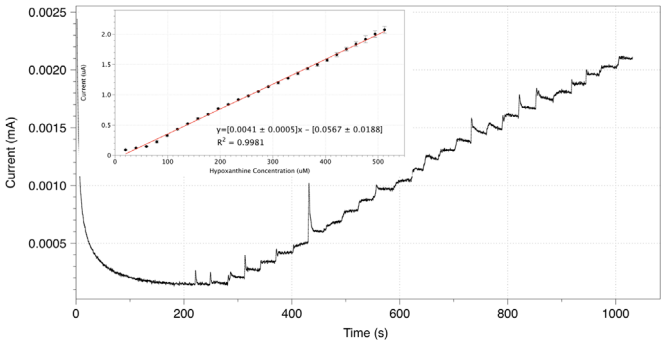

Fig. 4. Typical current-time response of the Nafion/XOD/TiO_2-G/GCE sensor to successive addition of 20 μM Hx into a stirred solution of 50 mM PBS at pH 7.0 at an applied potential of 0.8 V. Inset is the linear calibration curve of the biosensor.

Table 1
Recovery testing data in real meat samples using the Nafion/XOD/TiO_2-G/GCE sensor.

Sample	Storage Day	Hx Added (μM)	Hx Found (μM)	Recovery (%)
1	Day 0	0	21.1 ± 1.9	104.7 ± 2.7
		100	127.1 ± 4.3	
2	Day 7	0	111.3 ± 0.9	107.0 ± 1.9
		100	226.2 ± 4.5	

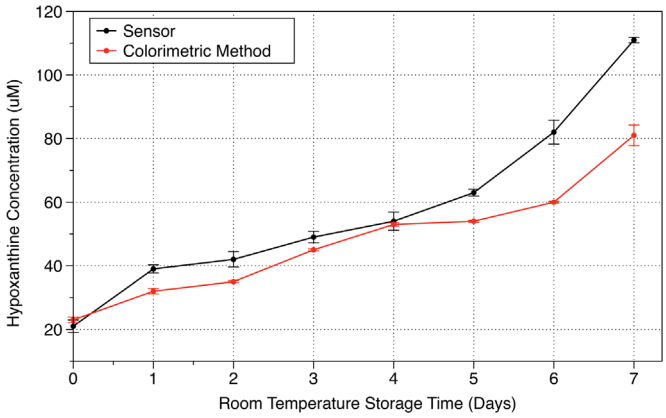

Fig. 5. Hx concentration in pork tenderloins stored at room temperature (22 ± 3 °C) as measured by fabricated sensor (black line) and by colorimetric method (red line). The values obtained by both methods has a correlation $r=0.9795$.

of the mentioned studies are lower compared to this work. The presence of the Nafion layer in the XOD/TiO_2-G/GCE surface may have caused the decreased response for lower concentrations of Hx due to the slow substrate diffusion through the Nafion layer. Nevertheless, the detection limit of the sensor in this study is better compared to the detection limit (200 μM) of mediated amperometric Hx sensors (Nguyen and Luong, 1993).

Overall, the developed Nafion/XOD/TiO_2-G/GCE sensor demonstrated advantages such as better sensitivity and linear range, as well as simplicity in the biosensor preparation. The analytical performance is within the range of Hx concentrations in meat samples stored at room temperature (Devi et al., 2013b). Thus, the sensor can be used to reliably evaluate the freshness of meat at room temperature.

3.7. Repeatability, reproducibility, stability, and recovery

The repeatability and the reproducibility of the biosensor were determined at the Hx concentration of 200 μM. The relative standard deviation of current response for five determinations for the same biosensor was 4.3% indicating good repeatability. The relative standard deviation of current response at five independently prepared biosensors was 3.8% indicating good reproducibility of the biosensor preparation. When the biosensor was stored at 4 °C immersed in 50 mM PBS, and used five times every five days for 30 days, the enzyme electrode retained about 77% of its initial activity after the 10th day and retained about 50% of its initial activity from the 15th to the 30th day. XOD was found to be one of the most fragile and henceforth short living enzymes (Coughlan and Johnson, 1979; Dodevska et al., 2010). The review paper of Pundir (Pundir and Devi, 2014) reported the useful lifetime of XOD based biosensors from as low as 4 days (30% loss of activity) to as high as 100 days (40% loss of activity).

Recovery testing was carried out to determine the accuracy and precision of the biosensor when applied to real meat samples. The values measured for three determinations were summarized in Table 1. The % recoveries of the biosensor were close to 100% indicating a satisfactory recovery data.

3.8. Testing on meat samples

To verify the applicability of the fabricated biosensor to the assessment of meat freshness, the sensor was used to determine the Hx concentration in pork tenderloins stored at room temperature for 7 days. Pork tenderloins were selected since in the study of (Rong et al., 2015), it was found that pork tenderloins contain the highest amount of Hx and the highest amount of total purine compared to other parts of pork.

The Hx concentration in pork tenderloins increases with storage days as measured by the fabricated sensor (Fig. 5). The increase in detected Hx concentration correlates with the physical indicators pertaining to meat that is no longer fresh and fit for human consumption. To test the accuracy, the present method was compared with the results obtained by standard enzymatic colorimetric method. Measurements from both methods has a correlation coefficient $r=0.9795$ which indicates good and acceptable analytical performance of the fabricated biosensor in real meat samples. Additionally, a t-test yields a p value greater than 0.05, indicating that there is no significant difference between the measurements obtained by the fabricated sensor and by colorimetric method.

4. Conclusions

In summary, our results showed that the hydrothermally synthesized TiO_2-G nanocomposite provided a favorable microenvironment for the direct electrochemistry of XOD and can be used as new platform for the construction of an enzymatic amperometric sensor. The fabricated Nafion/XOD/TiO_2-G/GCE sensor exhibited good electro catalytic activity towards Hx with a linear range of 20–512 μM, LOD of 9.5 μM, and sensitivity of 4.1 nA/μM. The biosensor also exhibited good selectivity and can effectively detect Hx in real meat samples.

Acknowledgement

This research project was supported by the United States Agency for International Development (USAID) through the USAID-STRIDE Graduate Scholarship Program, and the Philippine Government's Department of Science and Technology-ASTHRDP Scholarship Grant.

Appendix A. Supplementary material

Supplementary data associated with this article can be found in the online version at http://dx.doi.org/10.1016/j.bios.2016.03.041.

References

Ag, L., Manso, J., Paloma, Y., Pingarr, M., 2006. Sens. Actuators B Chem. 113, 272–280.
Akaoka, I., Nishizawa, T., Nishida, Y., 1975. Biochem. Med. 14, 285–289.
Akhavan, O., Ghaderi, E., 2009. J. Phys. Chem. C 113, 20214–20220.
Amigo, J.M., Coello, J., Maspoch, S., 2005. Anal. Bioanal. Chem. 382, 1380–1388.
Anjusree, G.S., Nair, A.S., Nair, S.V., Vadukumpully, S., 2013. RSC Adv., 12933–12938.
Baş, S.Z., Gülce, H., Yildiz, S., 2014. Int. J. Polym. Mater. 63, 476–485.
Chen, P., McCreery, R.L., 1996. Anal. Chem. 68, 3958–3965.
Chen, Y., Wang, J., Liu, Z.-M., 2012. Chin. J. Anal. Chem. 40, 1772–1779.
Cooper, N., Khosravan, R., Erdmann, C., Fiene, J., Lee, J.W., 2006. J. Chromatogr. B 837, 1–10.

Coughlan, M.P., Johnson, D.B., 1979. Biochem. Soc. Trans. 7, 18–21.
Dave, D., Ghaly, A.E., 2011. Am. J. Agric. Biol. Sci. 6, 486–510.
Devi, R., Batra, B., Lata, S., Yadav, S., Pundir, C.S., 2013a. Process Biochem. 48, 242–249.
Devi, R., Thakur, M., Pundir, C.S., 2011a. Biosens. Bioelectron. 26, 3420–3426.
Devi, R., Yadav, S., Nehra, R., Pundir, C.S., 2013b. Int. J. Biol. Macromol. 62, 629–635.
Devi, R., Yadav, S., Pundir, C.S., 2012. Analyst 137, 754.
Devi, R., Yadav, S., Pundir, C.S., 2011b. Biochem. Eng. J. 58–59, 148–153.
Dodevska, T., Horozova, E., Dimcheva, N., 2010. Cent. Eur. J. Chem. 8, 19–27.
Dong, P., Wang, Y., Guo, L., Liu, B., Xin, S., Zhang, J., Shi, Y., Zeng, W., Yin, S., 2012. Nanoscale 4, 4641.
Fan, Y., Huang, K., Niu, D., Yang, C., Jing, Q., 2011a. Electrochim. Acta 56, 4685–4690.
Fan, Y., Lu, H.-T., Liu, J.-H., Yang, C.-P., Jing, Q.-S., Zhang, Y.-X., Yang, X.-K., Huang, K.-J., 2011b. Colloids Surf. B. Biointerfaces 83, 78–82.
Feng, C., Xu, G., Liu, H., Lv, J., Zheng, Z., Wu, Y., 2013. J. Solid State Electrochem. 18, 163–171.
Galgano, F., Favati, F., Bonadio, M., Lorusso, V., Romano, P., 2009. Food Res. Int. 42, 1147–1152.
Gil, L., Barat, J.M., Baigts, D., Martínez-Máñez, R., Soto, J., Garcia-Breijo, E., Aristoy, M.-C., Toldrá, F., Llobet, E., 2011. Food Chem. 126, 1261–1268.
Guo, J., Zhu, Y., Chen, Z., Liu, Q., Zhang, D., Moon, W.-J., Song, D.-M., 2012. RSC Adv. 2, 1356.
Guo, L., Yang, Z., Zu, B., Lu, B., Dou, X., 2016. RSC Adv. 6, 358–365.
Hernández-Cázares, A.S., Aristoy, M.-C., Toldrá, F., 2010. Food Chem. 123, 949–954.
Hu, S., 2000. Anal. Chim. Acta 412, 55–61.
Hu, Y., Li, F., Han, D., Niu, L., 2015. Biocompatible Graphene for Bioanalytical Applications. Springer Berlin Heidelberg, Berlin, Heidelberg.
Lawal, A.T., Adeloju, S.B., 2012a. Talanta 100, 217–228.
Lawal, A.T., Adeloju, S.B., 2012b. Food Chem. 135, 2982–2987.
Li, M., Liu, C., Xie, Y., Cao, H., Zhao, H., Zhang, Y., 2014. Carbon 66, 302–311.
Lim, H.N., Nurzulaikha, R., Harrison, I., Lim, S.S., Tan, W.T., Yeo, M.C., Yarmo, M.A., Huang, N.M., 2012. Ceram. Int. 38, 4209–4216.
Liu, M., Chena, S., Zhaoa, X., Ye, Y., Li, J., Zhua, Q., Zhao, B., Zhao, W., Huanga, X., Shen, J., 2013. Talanta, 536–542.
Luong, J.H.T., Male, K.B., 1992. Enzym. Microb. Technol. 14, 125–130.
Mao, L., Xu, F., Xu, Q., Jin, L., 2001. Anal. Biochem. 292, 94–101.
Metz, S., Thiel, W., 2009. J. Am. Chem. Soc. 131, 14885–14902.
Muduli, S., Lee, W., Dhas, V., Mujawar, S., Dubey, M., Vijayamohanan, K., Han, S.-H., Ogale, S., 2009. ACS Appl. Mater. Interfaces 1, 2030–2035.
Murugan, A.V., Muraliganth, T., Manthiram, A., 2010. Chem. Mater. 22 2692–2692.
Nguyen, A.-L., Luong, J.H.T., 1993. Biosens. Bioelectron. 8, 421–431.
Nicholson, R.S., 1965. Anal. Chem. 37, 1351–1355.
Önal, A., 2007. Food Chem. 103, 1475–1486.
Öztürk, F.Ö., Erden, E., Kaçar, C., Kiliç, E., 2014. Acta Chim. Slov., 19–26.
Pundir, C.S., Devi, R., 2014. Microb. Technol 57, 55–62.
Qiu, J., Lai, C., Wang, Y., Li, S., Zhang, S., 2014. Chem. Eng. J. 256, 247–254.
Raj, M.A., John, S.A., 2013. Anal. Chim. Acta 771, 14–20.
Rodrigues, C.G., Wedd, A.G., Bond, A.M., 1991. J. Electroanal. Chem. 312, 131–140.
Rong, S., Zou, L., Zhang, Y., Zhang, G., Li, X., Li, M., Yang, F., Li, C., He, Y., Guan, H., Guo, Y., Wang, D., Cui, X., Ye, H., Liu, F., Pan, H., Yang, Y., 2015. Food Chem. 170, 303–307.
Shan, D., Wang, Y.-N., Xue, H.-G., Cosnier, S., Ding, S.-N., 2009. Biosens. Bioelectron. 24, 3556–3561.
Shao, Y., Wang, J., Wu, H., Liu, J., Aksay, I.A., Lin, Y., 2010. Electroanalysis 22, 1027–1036.
Shen, J., Yan, B., Shi, M., Ma, H., Li, N., Ye, M., 2011. J. Mater. Chem. 21, 3415.
Tang, L., Wang, Y., Li, Y., Feng, H., Lu, J., Li, J., 2009. Adv. Funct. Mater. 19, 2782–2789.
Timur, S., Wang, J., Telefoncu, A., 2004. Electrochem. Commun. 6, 913–916.
Torres, A.C., Ghica, M.E., Brett, C.M.A., 2013. Anal. Bioanal. Chem. 405, 3813–3822.
Urban, G., 2013. Designing Receptors for the Next Generation of Biosensors. Springer Berlin Heidelberg, Berlin, Heidelberg.
Uzunoglu, A., Zhang, H., Andreescu, S., Stanciu, L.A., 2015. J. Mater. Sci. 50, 3750–3762.
Vallé, M., Malle, P., Bouquelet, S., 1998. J. AOAC Int. 81, 571–575.
Vasconcelos, D.C.L., Costa, V.C., Nunes, E.H.M., Sabioni, A.C.S., Gasparon, M., Vasconcelos, W.L., 2011. Mater. Sci. Appl. 02, 1375–1382.
Vinci, G., Antonelli, M., 2002. Food Control 13, 519–524.
Wang, J., Zhou, Y., Xiong, B., Zhao, Y., Huang, X., Shao, Z., 2013. Electrochim. Acta 88, 847–857.
Watanabe, E., Endo, H., Hayashi, T., Toyama, K., 1986. Biosensors 2, 235–244.
Weeranantanaphan, J., Downey, G., Allen, P., Sun, D.-W., 2011. J. Infrared Spectrosc. 19, 61.
Yam, Y., Kataho, N., Watanabe, O.M., Nakamura, T., Asad, Y., 1995. Food Chem., 52.
Yano, Y., Yokoyama, K., Tamiya, E., Karube, I., 1996. Anal. Chim. Acta 320, 269–276.
Yao, T., 1993. Anal. Chim. Acta 281, 323–326.
Yu, Y., Yang, Y., Gu, H., Yu, D., Shi, G., 2013. Anal. Methods 5, 7049.
Zhang, H., Lv, X., Li, Y., Wang, Y., Li, J., 2010. ACS Nano 4, 380–386.
Zhang, J., Lei, J., Pan, R., Xue, Y., Ju, H., 2010. Biosens. Bioelectron. 26, 371–376.
Zhang, L., Lei, J., Zhang, J., Ding, L., Ju, H., 2012. Analyst 137, 3126.
Zhou, H., Xu, Y., Chen, T., Suzuki, I., Li, G., 2006. Anal. Sci. 22, 337–340.
Zou, F., Yu, Y., Cao, N., Wu, L., Zhi, J., 2011. Scr. Mater. 64, 621–624.

Please cite this article as: Albelda, J.A.V, et al., Biosensors and Bioelectronics (2016), http://dx.doi.org/10.1016/j.bios.2016.03.041